RSC Advances




ROYAL SOCIETY OF CHEMISTRY

www.rsc.org/advances

# The Fibrous Membrane Electrospun from Suspension Polymerized Resultant of Styrene and Butyl acrylate for Oil-Water Separation

L. Q. Ning[a], N. K. Xu[*b], R. Wang[a] and Y. Liu[a]

a State Key Laboratory of Separation Membranes and Membrane Processes, School of Textiles, Tianjin Polytechnic University, 300387 Tianjin, China

b State Key Laboratory of Separation Membranes and Membrane Processes, School of Material Science and Engineering, Tianjin Polytechnic University, 300387 Tianjin, China



[*]Corresponding author: Dr. Naiku Xu. E-mail: xunaiku@tjpu.edu.cn, Tel: +86-22-83955794, Fax: +86-22-83955055

**Abstract**: In this work, several polymers were synthesized via suspension polymerization when styrene and butyl acrylate were used as rigid unit and flexible unit, respectively, and the prepared polymers were then electrospun into the fibrous membranes with good low-temperature flexibility. The obtained fibrous membranes had perfect hydrophobicity and lipophilicity, and their water contact angle approached 155.0° as the fibrous membranes were wetted by sunflower oil, thus the fibrous membranes possessed good capability to separated oil from water. We researched the effect of initial oil content, extrusion rate, and the position of oil-water interface on their oil-water separation capability, and the corresponding results showed that the maximum oil removal efficiency could reach 97.3%, and oil removal efficiency was still up to 74.2% as the fibrous membrane was used for the seventh time, additionally, the fibrous membranes could make the O/W emulsion clear via oil absorption from water. In addition, we also investigated the other aspects of the fibrous membranes through the corresponding instruments.

**Keywords**: styrene; butyl acrylate; suspension polymerization; electrospun fibrous membrane; oil-water separation

## Introduction

In recent years, with the development of industry, oily sewage, waste liquids, and industrial accidents such as oil leakage from oil tanker and oil ship have caused serious environmental pollution since oily organic compounds have the characteristics of persistence, bioaccumulation, half volatility, long distance migration, and high toxicity. For the sake of protecting our environment and human health, as well as oil recovery, it is urgent to develop and produce the novel materials that can be used to absorb and separate oil from water.

For a long time, people used these materials such as kapok fiber [1, 2] and polypropylene non-woven fabric [3, 4] to absorb oil. Kapok fiber and polypropylene non-woven fabric usually have these weaknesses such as poor heat or cold resistance, slow absorption rate, poor oil-water selectivity, and weak oil retention, etc., thus they cannot meet the requirements of oil recovery and environmental protection. In order to approach the target of oil absorption and separation from water, a kind of functional polymer called highly oil-absorptive resin has been widely researched. The highly oil-absorptive resin was firstly synthesized in the United States in 1966. Since then, the highly oil-absorptive resin got a fast development. The resin possesses a lot of advantages including good temperature resistance, broad applicability, excellent oil-water selectivity, good oil retention under pressure, and store and transport convenience [5], thus the above-mentioned materials such as kapok fiber and polypropylene non-woven fabric were replaced by the highly oil-absorptive resin in the field of oil absorption and separation. The highly oil-absorptive resin is a kind of polymer synthesized from lipophilic monomers and crosslinking agent, and it has a three-dimensional network structure, thus the oils cannot dissolve it but be wrapped by its network. Among them, the resin synthesized using acrylate and methyl acrylate as lipophilic monomers is the main product because of wide source of raw material and mature polymerization technique [6-9].

In spite of relatively high oil absorbency and good oil-water separation performance, the highly oil-absorptive resin is

generally granular in shape, and its specific surface area is not large enough. In this instance, it is very difficult for the highly oil-absorptive resin to be recycled and reused, and the highly oil-absorptive resin has very slow oil absorption rate. Therefore, the electrospun fibrous membranes with good reusability and high specific surface area have attracted the attention of researchers [10]. Polystyrene, as a hydrophobic and electrospinnable polymer, has long been used to prepare oil-absorptive material via electrospinning [11-13]. Qiu et al. used waste polystyrene as raw material to prepare fibrous membrane via electrospinning, and its maximum oil absorbency for motor oil, ethylene glycol, peanut oil, and diesel oil was 124g/g, 98g/g, 105g/g, and 48g/g, respectively [14]. Lee et al. used steel net to collect electrospun polystyrene nanofibers, and prepared a superhydrophobic and superoleophilic composite membrane by one-step deposition method. They found that the membrane could selectively separate oil from water [15]. However, the electrospun polystyrene fibrous membrane has a cotton-like appearance, and its weight is extremely light, thus it exhibits extremely low strength and small elongation at break. Due to these poor mechanical properties, the electrospun polystyrene fibrous membrane cannot be reused after oil absorption. In addition, the rigidity of polystyrene makes its fibrous membrane brittle at low temperature, so the electrospun polystyrene fibrous membrane has poor adaptability for practical application. Hence, one applicable way is needed to improve the properties of the electrospun polystyrene fibrous membrane.

It is well known that poly(butyl acrylate) is a very ductile and sticky polymer (an elongation of 2000% at break) with low glass transition temperature and good low-temperature flexibility [16]. Additionally, poly(butyl acrylate) has very good affinity for oils. Thereby we used butyl acrylate as comonomer to copolymerize with styrene in this work, and expected the fibrous membrane electrospun from the suspension polymerized resultant of styrene and butyl acrylate had similar function to polystyrene fibrous membrane but had better low-temperature flexibility in comparison with polystyrene fibrous membrane.

## Experimental section

### Materials

Styrene (St) was purchased from Tianjin Fuchen Chemical Reagents Factory and used as received. N-butyl acrylate (BA) was supplied by Tianjin Guangfu Fine Chemical Research Institute and used as received. Poly (vinyl alcohol) (PVA) was supplied by Hunan Xiangwei Co., Ltd and used after washing by water and drying in a vacuum oven. Benzoyl peroxide (BPO) was obtained from China National Pharmaceutical Group Corp. Shanghai Chemical Reagent Co., Ltd and used as received. N, N-dimethylformamide (DMF) was supplied by Tianjin Guangfu Science and Technology Development Co., Ltd and used without any treatment. Absolute ethyl alcohol was offered by Tianjin Fengchuan Chemical Reagent Technologies Co., Ltd and used as received. Pump oil was purchased from Tianjin Shifang Chemical Industry Co., Ltd and used directly. Sunflower oil was supplied by Kerry Grain and Oil (Tianjin) Co., Ltd and used directly. Hexyl hydride was obtained from Tianjin

Fengchuan Chemical Reagent Technologies Co., Ltd and used without any treatment. Hydrochloric acid was purchased from Beijing Beihua Chemical Plant and used directly. Anhydrous sodium sulfate was supplied by Tianjin Fengchuan Chemical Reagent Technologies Co., Ltd and used directly. Sodium dodecyl sulfate (SDS) was offered by Tianjin Zhiyuan Chemical Reagent Co., Ltd and used as received.

**Polymer synthesis**

A solution was firstly prepared by stirring 2.25g PVA and 100ml deionized water in a beaker at 80°C, and the solution was then cooled down to room temperature. Thereafter, BPO whose mass was equal to 0.5% of the total mass of St and BA was mixed with the mixture of St and BA with a total volume of 150ml in another beaker at room temperature, and another solution was subsequently obtained by stirring BPO, St, and BA in the beaker. The mass fraction of BA in the mixture of St and BA was assigned to 0, 10, 20, 30, 40, 50, or 60%, and the mass fraction of St in the mixture of St and BA was correspondingly equal to 100, 90, 80, 70, 60, 50, or 40%. Then, the above-prepared two solutions and 350ml deionized water were stirred to react at 85°C for 3 hours under nitrogen atmosphere in a three-neck flask, and then the reaction system was maintained for another 3 hours at 95°C under nitrogen atmosphere. After separating from the aqueous solution of PVA via vacuum filtering, the resultant was washed firstly by hot water, and then washed by deionized water. Finally, seven kinds of polymers were obtained through drying in a vacuum oven at 33°C. The polymers that were prepared when the mass fraction of BA in the mixture of St and BA equaled to 0, 10, 20, 30, 40, 50, or 60% were labeled as P1, P2, P3, P4, P5, P6, and P7, respectively.

**NMR Analysis**

An Avance 300MHz (Bruker Corp., Germany) nuclear magnetic resonance (NMR) spectrometer was used to analyze the composition of the synthesized polymers. The test was performed at a resonance frequency of 300Hz for $^{1}H$ at room temperature. The corresponding spectra was obtained by using deuterated chloroform ($CDCl_3$) as solvent, and chemical shifts were referenced to tetramethylsilane (TMS).

**GPC analysis**

In order to analyze the molecular weight and molecular weight distribution of the synthesized polymers, a Viscotek gel permeation chromatography (GPC) system (Malvern Instruments Ltd, England) was used, and its column temperature was 35.0°C. Polystyrene was used as the standard sample, and chromatographically pure tetrahydrofuran (THF) was used as solvent. The flow rate of the THF solution of the synthesized polymer was 1.000ml/min, and its injection volume was 100.0μl.

**Fibrous membrane preparation**

The above-synthesized polymers P1 to P7 were respectively dissolved in DMF to prepare spinning solutions with a

mass concentration of 20%. Each solution was firstly placed in a 10ml plastic syringe, and the syringe was then connected with a metallic needle having an inner diameter of 0.6mm. Then the syringe was fixed horizontally on a 789100C microinjection pump (Cole-Parmer Instrument Company, America) which was used to provide an extrusion rate of 0.8ml/h for the spinning solution. Thereafter a DW-P303-1ACD8 DC high voltage power supply (Tianjin Dongwen High Voltage Co., Ltd, China) was used to generate a potential difference of 15kV between the needle and an aluminum foil-covered grounded collector that was positioned at the distance of 20cm away from the needle tip and rotated at a speed of 200r/min. The electrospinning was performed at 25°C, and relative humidity was maintained at 40% by using a dehumidifier. When the spinning process was carried out for 30h, the fibrous membrane was obtained, and the membranes which were fabricated from the polymers P1, P2, P3, P4, P5, P6, and P7 were labeled as 1*, 2*, 3*, 4*, 5*, 6*, and 7*, respectively.

**DMA analysis**

The above-synthesized polymers were respectively dissolved in DMF to prepare spinning solutions with a mass concentration of 20%. After vacuum defoamation, each solution was spun into fibers via wet spinning, as shown in Figure 1. The spinning solution was firstly placed into a beaker, and the spinning solution was subsequently pumped into a spinneret with a flow rate of 0.3ml/min through a BT100L peristaltic pump (Baoding Lead Fluid Technology Co., Ltd, China). Thereafter, the spinning solution was extruded from the holes and transformed into spinning threads. After solidification in water bath via double diffusion and drying in a vacuum oven at 33°C, as-spun fibers were obtained. The as-spun fibers were labeled as 1#, 2#, 3#, 4#, 5#, 6#, and 7# according to its polymer. In addition, the spinneret had eight holes, and the diameter of each hole was 0.8mm. Finally, the thermomechanical properties of the as-spun fibers were researched by a DMA242C dynamic thermomechanical analyzer (Netzsch, Germany). The test was performed within the temperature range of -65°C to 200°C at a heating rate of 5°C/min and a frequency of 1Hz.

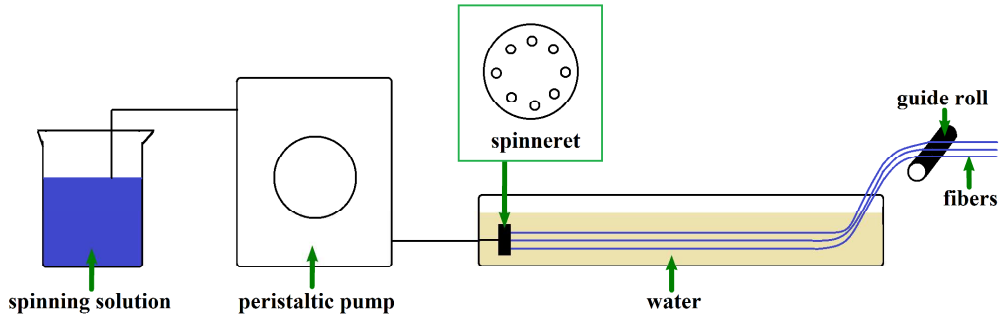


**Figure 1.** a sketch map of wet spinning

**XPS analysis**

The surface elements of the fibrous membranes were analyzed on a K-Alpha X-ray photoelectron spectrometer (XPS) (Thermofisher Scienticfic Company, America), and monochromatized Al Kα radiation was used to probe the sample. The

spot size was 400μm, analyzer mode was CAE: pass energy 50.0eV, and energy step size was 0.100eV.

**TG analysis**

The thermal stability of the fibrous membranes was analyzed on a STA 409PC thermogravimetric analyzer (TG) (Netzsch, Germany). The measurement was performed from ambient temperature to 600°C at a heating rate of 10°C/min under nitrogen atmosphere.

**DSC analysis**

The thermal behaviors of the fibrous membranes were analyzed on a DSC 200F3 differential scanning calorimeter (DSC) (Netzsch, Germany) equipped with a cooling device. The measurement was performed from 20°C to 250°C under nitrogen atmosphere at a heating rate of 10°C/min.

**XRD analysis**

The crystallization behaviors of the fibrous membranes were researched on an AXS DS discover with GADDS X-ray diffractometer (XRD) (Bruker, Germany). Diffractometer with copper cathode was operated in reflectance mode at Cu-$K_{\alpha 1}$ wavelength of 1.5406Å, 40kV and 40mA. The measurement was performed within the 2-theta scale of 10° to 45° at a scanning rate of 4°/min.

**FESEM observation**

The surfaces of the fibrous membranes were firstly coated with gold by an electro-deposition method, and then their surface morphologies were observed on a NOVA NANOSEM 230 (FEI, America) field emission scanning electron microscope (FESEM) at an accelerating voltage of 15.0kV.

**Hydrophobicity and lipophilicity test**

The static water (or sunflower oil) contact angle of the fibrous membrane was measured by the liquid-drop method, and performed on a DSA100 contact angle tester (Kruss, Germany) equipped with a high-resolution CCD camera at room temperature. The reported value in this work was the average contact angle of at least six droplets deposited at different positions of the sample surface.

**Oil-water separation test**

The fibrous membrane was gently stripped from the aluminum foil after treatment for 1h in the aqueous solution of ethanol with a volume concentration of 1% at 30°C, and then the fibrous membrane was installed in a membrane holder after air drying. The mixture of pump oil and deionized water with a total volume of 10ml was firstly sucked into a 30ml syringe, and then the syringe was horizontally fixed on a LSP01-2A injection pump (Baoding Longer Pump Co., Ltd, China). Thereafter, the syringe was connected to the membrane holder containing the fibrous membrane, and a stainless steel needle was fasten to the other end of the membrane holder, additionally, a small bottle was positioned at the bottom of

the needle to collect the filtrate. The effect of initial oil content, extrusion rate, and the position of oil-water interface on oil removal efficiency was determined in this section. The test would be stopped at a certain time when water flowed into the bottle, and then the fibrous membrane was observed by a BX51 polarized optical microscope (Olympus Corporation, Japan). In addition, in order to analyze oil removal efficiency, the residual pump oil in the syringe was determined via extraction. Firstly, the residual mixture in the syringe was transferred to a 60ml separatory funnel. 25ml n-hexane was used to clean the syringe, and the washing liquid was also transferred to the separatory funnel. Secondly, a suitable amount of hydrochloric acid was added into the separatory funnel to acidize the liquid, and 0.1~0.3g anhydrous sodium sulfate was also put into the separatory funnel. Thirdly, the liquid in separatory funnel was divided into two different parts after full oscillation, constant deflation, and standing for a long time, and then the lower-layer liquid was abandoned, and the upper-layer liquid was diluted *N* times with n-hexane. A UV1901 UV-Vis spectrophotometer (Shanghai Youke Instrument Co., Ltd, China) was applied to measure the absorbance of the diluted liquid, and the concentration of pump oil in the diluted liquid could be calculated via the linear equation of the standard curve, as shown in Figure 2. Finally, the mass of residual pump oil in the syringe was calculated according to the equation (1), and oil removal efficiency was determined from the equation (2).

The capability of the fibrous membrane to separate emulsified pump oil from water was tested as the following procedures. 0.2ml pump oil, 3.8ml water, and SDS whose mass was equal to 0.8% of the total mass of pump oil and water were mixed together to form milky O/W emulsion. Then 2ml emulsion was sucked into a 10ml syringe, and the syringe was horizontally fixed on the injection pump. Thereafter, the syringe was connected to the membrane holder containing the fibrous membrane 3*, and a stainless steel needle was fastened to the other end of the membrane holder, additionally, a small bottle was positioned at the bottom of the needle to collect the filtrate. An extrusion rate of 4ml/h was used to make the emulsion pass through the fibrous membrane, and this process would not be stopped until all the emulsion flowed from the syringe. Finally, we adopted the extraction method mentioned above to analyze the mass of residual pump oil in the filtrate.

$$m_1 = C \times N \times V \times 10^{-4} \quad (1)$$

Where $m_1$ is the mass of residual pump oil in the syringe, g; *C* is the concentration of pump oil in the diluted liquid, mg/l; *N* is the dilution ratio, 100; *V* is the volume of n-hexane, 25ml.

$$E = \frac{m_0 - m_1}{m_0} \times 100\% \quad (2)$$

Where *E* is oil removal efficiency; $m_0$ is the mass of initial pump oil in the syringe, g; $m_1$ is the mass of residual pump oil in the syringe, g.

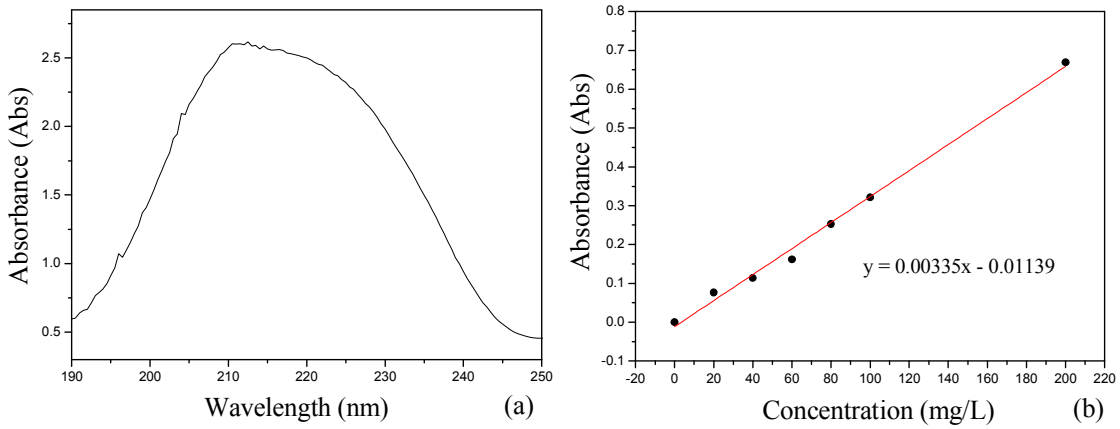


**Figure 2.** UV-Vis spectra of pump oil/n-hexane solution (a) and its standard curve at 211.0nm (b)

## Results and discussion

### Polymer composition

The $^{1}$H-NMR spectra of the synthesized polymers P1, P2, P3, P4, P5, P6, and P7 are depicted in Figure 4. The seven kinds of synthesized polymers all showed the peaks which were located at the band of 7.3ppm to 6.3ppm, and these peaks were the characteristic peaks of phenyl's protons (e, d) [17]. For the synthesized polymers P2, P3, P4, P5, P6, and P7, every one possessed an obvious peak located at 0.85ppm which was caused by the protons of -$CH_3$ from butyl acrylate structural unit (l) [18]. According to the calculation rule of copolymer composition, the protons of phenyl (e, d) and the protons of -$CH_3$ (l) could be used to calculate the content of styrene and butyl acrylate structure units in the synthesized polymer [19, 20]. Therefore, we obtained the content of styrene and butyl acrylate structural units in the synthesized polymer, and the results are shown in Table 1. It could be clearly found that the content of styrene and butyl acrylate structural units in the synthesized polymer greatly approached the feed ratio of styrene to butyl acrylate.

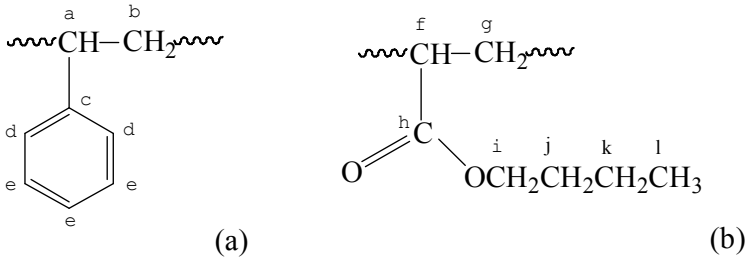


**Figure 3.** the chemical formulas of styrene structural unit (a) and butyl acrylate structural unit (b)

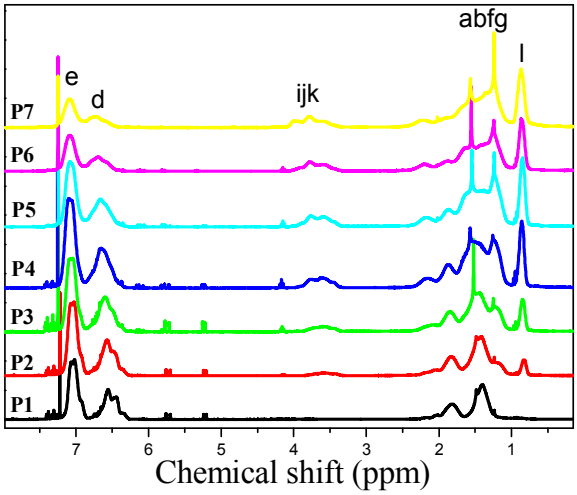


**Figure 4.** $^{1}$H-NMR spectra of the synthesized polymers P1, P2, P3, P4, P5, P6, and P7

**Table 1.** the content of styrene and butyl acrylate structural units in the corresponding polymer

| Structural unit | P1 | P2 | P3 | P4 | P5 | P6 | P7 |
|---|---|---|---|---|---|---|---|
| Styrene (%) | 100 | 90.1 | 82.0 | 72.0 | 63.7 | 54.4 | 42.0 |
| Butyl acrylate (%) | 0 | 9.9 | 18.0 | 28.0 | 36.3 | 45.6 | 58.0 |

**Mechanical properties**

The molecular weight of the synthesized polymers is depicted in Figure 5. It was clear that the molecular weight (Mw or Mn) of polystyrene was higher than that of the other polymers, and the Mw and Mn of the synthesized polymers exhibited a trend of decrease with increasing the mass fraction of BA in monomers. Additionally, it could be found from Table 2 that the polymer synthesized from the monomer mixture containing more St and less BA had a narrower distribution of molecular weight in comparison with polystyrene; however, for the polymer synthesized from the monomer mixture consisted of more BA and less St, it showed a relatively broader distribution of molecular weight. Since BA feed ratio could influence the molecular weight and molecular weight distribution of the synthesized polymers, it should have a great impact on mechanical properties of the fibrous materials prepared from the synthesized polymers. The fibers 1#, 2#, and 3# exhibited very strong brittleness, and the fiber 7# displayed very good stickiness, so it was very difficult to obtain the DMA spectra of these four fibers, and the tanδ and dL curves of the fibers 4#, 5#, and 6# are shown in Figure 6. It could be observed from Figure 6(a) that the fibers showed single damping peak, which indicated that all the suspension polymerized resultants were homogeneous. The damping peak represented α-shift, meaning that the chain segments of the corresponding polymer rotated around its main chain axis, thus we could determine glass transition temperature from the maximum of the damping peak. The glass transition temperatures of the fibers 4#, 5#, and 6# were equal to 91.9°C, 74.6°C, and 51.5°C, respectively. This phenomenon implied that the chain segments of the corresponding polymer had relatively

better mobility at low temperature with increasing BA feed ratio. In addition, the thermal deformation behaviors of the fibers 4#, 5#, and 6#, as shown in Figure 6(b), manifested that the temperature of initial deformation was about 80°C, 60°C, and 28°C for the fibers 4#, 5#, and 6#, and decreased with an increase in BA feed ratio. Thereby, we concluded that the fibrous material prepared from the suspension polymerized resultant of styrene and butyl acrylate had better low-temperature flexibility in comparison with the polystyrene fibrous material.

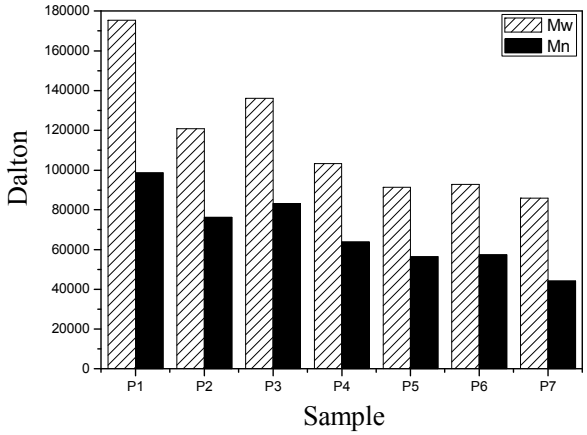


**Figure 5.** weight-average molecular weight (Mw) and number-average molecular weight (Mn)

**Table 2.** the polydispersity index (d) of the synthesized polymers

| Sample | P1 | P2 | P3 | P4 | P5 | P6 | P7 |
|---|---|---|---|---|---|---|---|
| d=Mw/Mn | 1.779 | 1.587 | 1.636 | 1.618 | 1.617 | 1.616 | 1.939 |

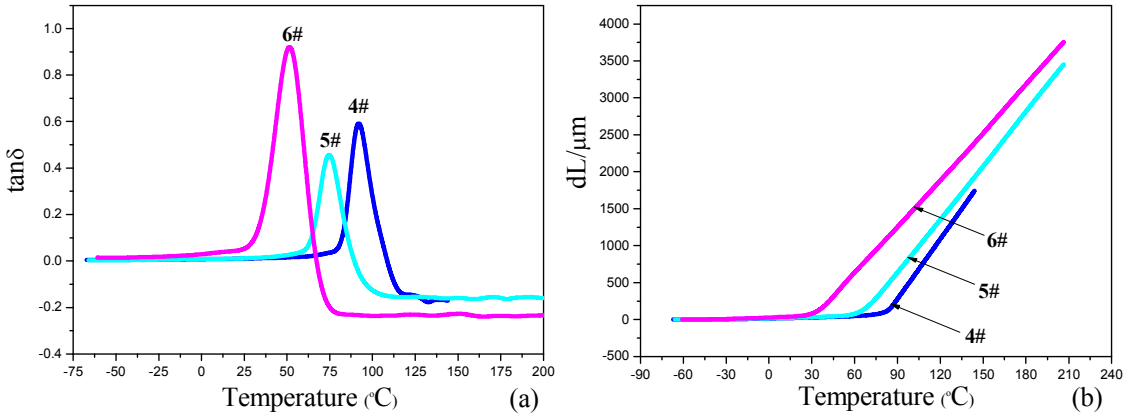


**Figure 6.** tanδ (a) and deformation (b) curves

**Surface elements**

It could be found from Figure 7(a) that C1s electrons were detected on the surfaces of all the samples. The XPS local spectra in Figure 7(b) showed that the sample 1* had an obvious peak centered at 284.5eV, corresponding to aliphatic carbons and aromatic carbons; additionally, a small hump (labeled by an uppercase A) also appeared at 291.3eV for the

sample 1*, corresponding to the π-π* shake-up transition of the aromatic ring [21, 22]. However, the above-mentioned small hump disappeared from the spectrum of the sample 5*, and another small hump centered at 288.3eV (labeled by an uppercase B) emerged, which was caused by the carbons of carbonyl groups of BA structural units [23, 24]. Besides, O1s electrons were also detected on the surfaces of the samples 2*, 3*, 4*, 5*, 6*, and 7*, which further proved that BA structural units did exist on the surfaces of these six samples. The signal of O1s electrons increased gradually with increasing BA feed ratio, which demonstrated that the number of BA structural units decreased with decreasing BA feed ratio. For the sample 1*, a very weak signal of O1s electrons was found, according to the literature [25], this signal should be caused by some contaminants such as water and organic molecules which were introduced during preparation or measurement.

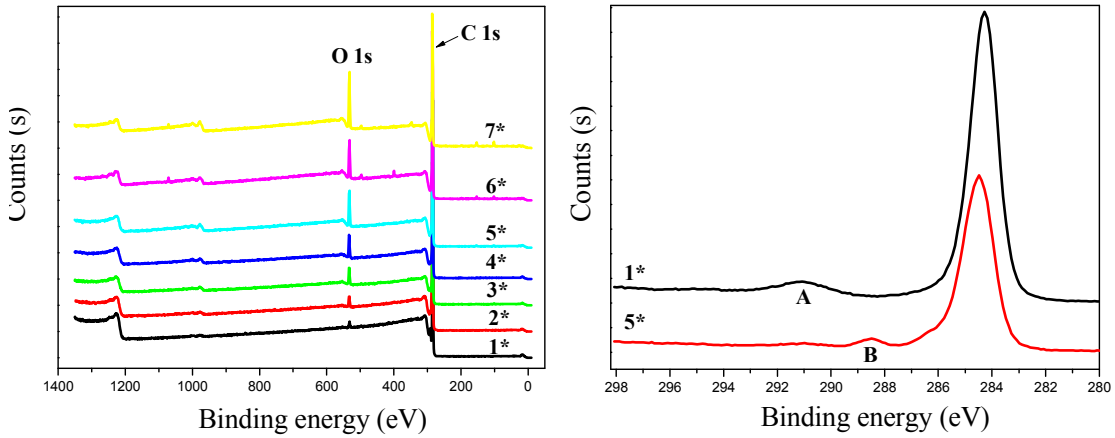


**Figure 7.** XPS full spectra (a) and C1s spectra (b)

**Thermal properties**

The thermogravimetric curves in Figure 8 revealed that every sample finished its weight loss with one step, indicating only one thermal decomposition process occurred within the range of test temperature. Every sample began to decompose at the temperature higher than 360°C. Based on the previous researches [26-31], the initial decomposition temperature was between 250°C to 320°C for poly(butyl acrylate) which was synthesized by using different initiators. According to the literatures [32, 33], polystyrene decomposed within the temperature range of 370°C to 450°C. However, there were no other decomposition processes below 360°C in DTG curves, thus the fibrous membranes didn't contain the component of poly(butyl acrylate). Taking the XPS results into consideration, we concluded that the suspension polymerized resultant of styrene and butyl acrylate was their copolymer. In addition, the temperature at which the maximal rate of weight loss happened decreased with increasing St feed ratio. It is well known that the chain segments formed by styrene structural units are only composed of saturated C-C bonds, and saturated C-C bonds can restrain the thermal motion of macromolecular chains [34], thus the incorporation of styrene structural units into copolymer can improve the thermal

stability of corresponding copolymer chains [35, 36]. However, the thermal stability of the sample became worse with increasing BA feed ratio. It is well known that the decomposition of polystyrene is mainly caused by end-chain break and random scission [37], and the scission of ester groups is the main cause for the decomposition of poly(butyl acrylate) [38]. The ester groups have relatively poor thermal stability, thus the sample's thermal stability got bad with the introduction of BA structural units into the corresponding copolymer.

The glass transition temperature of the sample 1* was about 111.2°C, in agreement with the values reported by the literatures [39, 40]. There was only one glass transition for the sample 2* or 3*, indicating that St was well copolymerized with BA in the process of suspension polymerization, and the glass transition temperature for the sample 2* or 3* was around 94.4°C or 85.6°C and lower than that of the sample 1*, in well accordance with the DMA results. However, there were no obvious glass transitions for the sample 4*, 5*, 6*, and 7* in DSC curves, this was caused by the poor sensitivity of DSC. DSC monitored the glass transition of polymer through detecting its thermal change, but DMA monitored glass transition via detecting polymer's deformation. Since the sample's deformation was more obvious than thermal change at the temperature near Tg, DSC had a poorer sensitivity to glass transition in comparison with DMA.

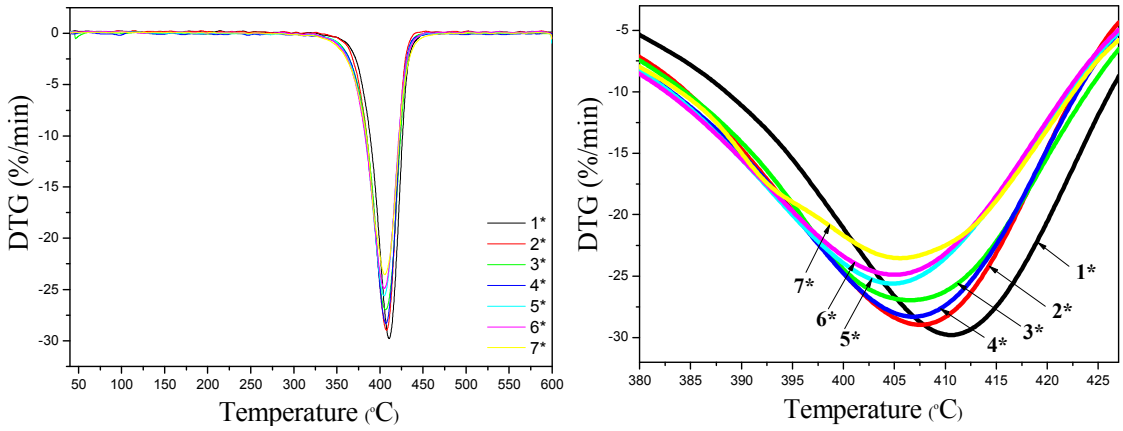


**Figure 8.** full DTG curves (a) and local DTG curves (b)

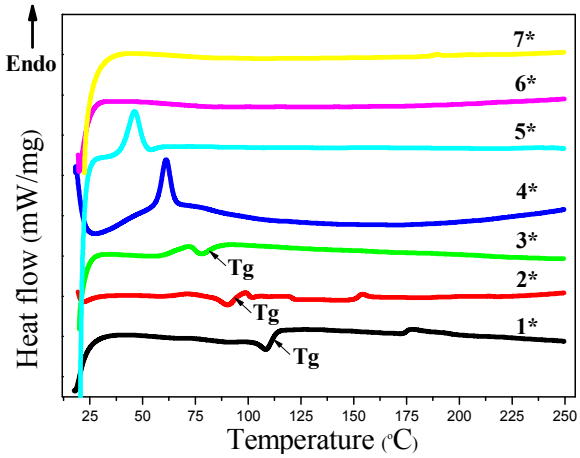


**Figure 9.** DSC curves of the electrospun fibrous membranes

**Crystallization behaviors**

The DSC curves of the samples 4* and 5*, as shown in Figure 9, possessed obvious endothermic peaks within the temperature range of 57.0~65.0°C and 40.3~50.9°C, respectively. A small endothermic peak within the temperature range of 59.6~76.8°C was also found in the DSC curve of the sample 3*. However, this endothermic peak was not found in the DSC curve of the sample 1*, 2*, 6*, or 7*. In addition, it could be found from Figure 10 that the sample 1* did not exhibit any sharp diffraction peaks, but showed a broad hump at the 2θ of around 20°, in well accordance with the semi-crystalline nature of polystyrene [41]. For the sample 2*, 6*, or 7*, this broad hump at the 2θ of around 20° was also found, but other sharp diffraction peaks were not found. Thereby, the prepared samples 1*, 2*, 6*, and 7* were amorphous. Additionally, two sharp diffraction peaks at the 2θ of 24° and 28° appeared in the XRD curves of the samples 4* and 5*, which was in well accordance with the DSC results and revealed that some ordered aggregation structures were formed in the samples 4* and 5* during electrospinning. Based on the above results, we considered that too much or too little BA could hardly improve the crystallinity of the suspension polymerized resultant of styrene and butyl acrylate during electrospinning, and only when a proper amount of BA was used to copolymerize with St, was their suspension polymerized resultant able to form ordered structure during electrospinning. Finally, the vertex temperatures of the endothermic peaks, as shown in Figure 9, were 71.8°C, 61.2°C, and 46.2°C for the samples 3*, 4*, and 5*, shifting to the low temperature area with increasing BA feed ratio, which suggested that the thermal stability of the formed ordered structure became weaker with increasing BA feed ratio. Taking the above thermal properties into consideration, we concluded that this weak thermal stability was caused by BA structural units.

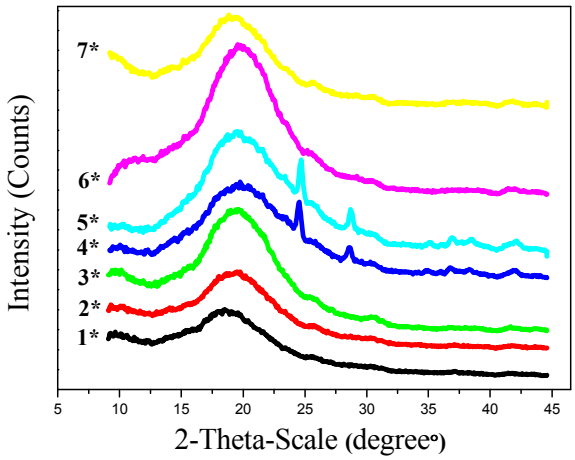


**Figure 10.** XRD patterns of the electrospun fibrous membranes

**Morphologies**

FESEM images of the electrospun samples are exhibited in Figure 11. The fibrous membranes prepared from seven polymer solutions with the same mass concentration of 20% had different morphologies. It could be found that the fibers in the samples 1*, 2*, and 3* were uniform in diameter and arranged in random orientation, and the corresponding magnified images showed that their surfaces were very smooth. The samples 4* and 5* both composed of beaded fiber. With an increase in BA feed ratio, significant changes occurred for the morphologies of the samples 6* and 7*. Some fiber could be found in the sample 6*, but all the fibers cohered together to form an integral structure. For the sample 7*, it completely lost fiber structure, and looked like a paper with a smooth surface. These phenomena demonstrated that BA had a great impact on the morphology of the sample electrospun from the corresponding suspension polymerized resultant of styrene and butyl acrylate. It was clear that this impact was caused by the viscidity and elasticity of BA structural units.

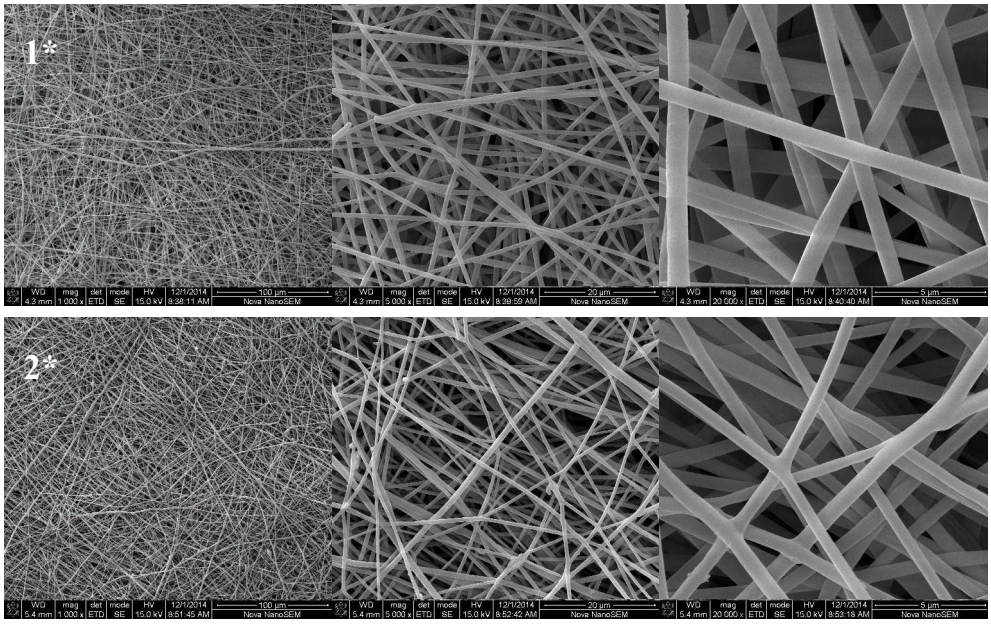

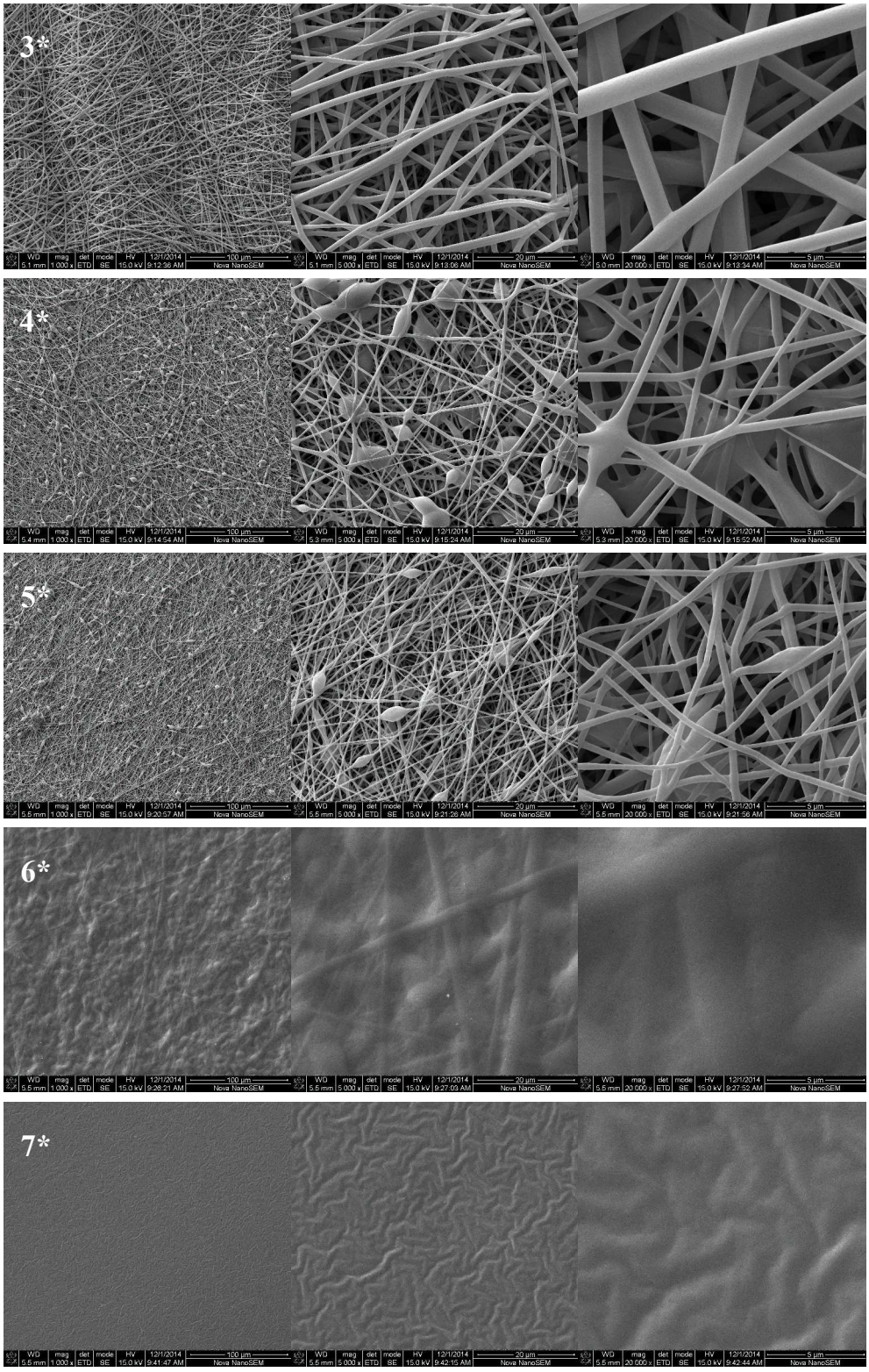


**Figure 11.** FESEM images of the electrospun fibrous membranes

**Hydrophobicity and lipophilicity**

The results of water contact angle (WCA) on the electrospun sample's surface are shown in Figure 12. Polystyrene is a

kind of polymer with low surface energy [42, 43]. Additionally, the polystyrene electrospun sample has rough surface due to the pore structure formed by the random arrangement of nano-micro fibers, and this surface can repel water [44, 45]. Based on these two reasons, the sample 1* had good hydrophobicity (WCA=134.0°±0.86°). When too little BA was used as comonomer, the corresponding samples such as 2* and 3* had similar WCA to the sample 1*. As too many BA was introduced into the polymerization system, the suspension polymerized resultants had a lot of polar ester groups, and the corresponding electrospun samples such as 4* and 5* had lower WCA in comparison with the samples 1*, 2*, and 3*. While BA feed ratio was increased continually, the electrospun samples 6* and 7* had very smooth surfaces, thus their WCA decreased greatly. However, all the samples were hydrophobic since their WCA was higher than 90°. In addition, owing to its affinity for oils as well as its loose and porous structure, the electrospun sample could completely absorb a droplet of sunflower oil within 1297 milliseconds, and then its oil contact angle reached 0°, as shown in Figure 13, which revealed that the electrospun samples had very good lipophilicity. Especially for the case that the electrospun sample was firstly immersed in oil and its WCA was subsequently measured, as shown in Figure 14, it could be found that its WCA approached 155°, exhibiting super-hydrophobicity, which provided possibility for further application in the field of oil-water separation.

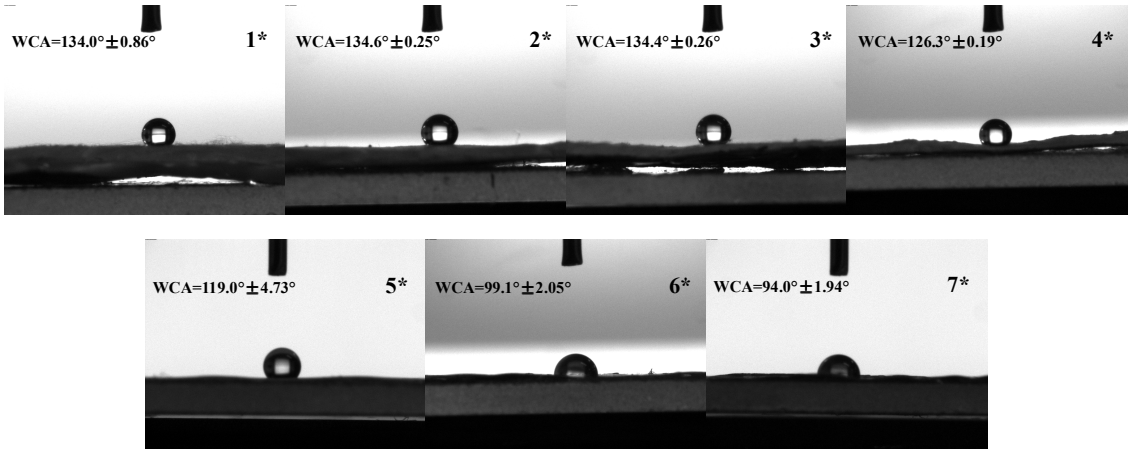


**Figure 12.** water contact angle of the electrospun fibrous membranes

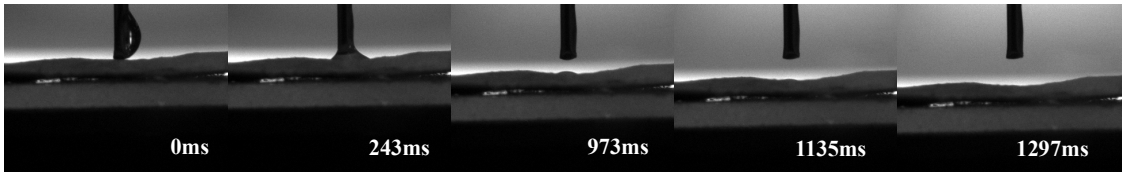


**Figure 13.** sunflower oil contact angle of the electrospun fibrous membrane 3*

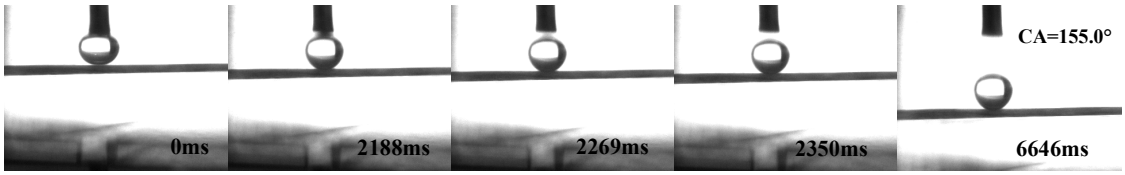


**Figure 14.** water contact angle of the electrospun fibrous membrane 5* in sunflower oil

**Oil-water separation performance**

The separation of oil-water mixture could be described by the following process. As soon as oil molecules encountered the fibrous membrane, they were immediately adsorbed by the fibrous membrane since the fibrous membrane had very good affinity for oil. However, water molecules could not be adsorbed by the fibrous membrane because water could hardly wet the fibrous membrane. Then an oil film was formed on the surface of the fibrous membrane. As the amount of oil on the fibrous membrane's surface increased, some oil droplets passed through the fibrous membrane under the action of driving force provided by the injection pump; however, water could not pass through the fibrous membrane due to the water repellency of the oil film. In this instance, oil was separated from water. For oil-water separation, there were many factors that could affect the separation process.

Firstly, we measured the influence of initial oil content on oil removal efficiency. From Figure 15 we noted that as initial oil content increased from 44 to 440g/l, oil removal efficiency rose gradually, and then tended to be stable. It was clear that the more oil in the oil-water mixture, the better oil film the surface of the fibrous membrane was covered with; thus water could be completely repelled by the oil film and hardly pass through the fibrous membrane, then for the oil-water mixture containing more oil, oil removal efficiency reached 97.3%. This meant that almost all the oil was separated from water.

Secondly, we investigated the influence of extrusion rate on oil removal efficiency. As Figure 16(a) shows, oil removal efficiency firstly increased and then decreased with an increase in extrusion rate from 2ml/h to 8ml/h, and the highest oil removal efficiency appeared at 6ml/h. With increasing extrusion rate, more oil passed through the fibrous membrane since the driving force imposed on oil became larger, leading to higher oil removal efficiency. However, as extrusion rate exceeded 6ml/h, we could find from Figure 16(b) that some structural defects appeared for the fibrous membrane, and water could pass through these weak regions, then oil removal efficiency reduced.

Thirdly, we researched the influence of the position of oil-water interface on oil removal efficiency, and the results are depicted in Figure 17. In this section, the syringe with eccentric outlet was used to make oil-water interface lower than the bottom of its outlet during separation; while the syringe with centered outlet was applied to make oil-water interface higher than the top of its outlet. For the syringe with eccentric outlet, oil was the first substance to contact the fibrous

membrane, and the fibrous membrane was subsequently wetted by oil, then the oil film formed on the fibrous membrane's surface could greatly repel water, thus oil removal efficiency reached up to 89.0% or 96.7% when initial oil content was equal to 176g/l or 440g/l. However, as the syringe with centered outlet was used, due to the absence of oil film, water could also pass through the fibrous membrane, thus oil removal efficiency was only 14.9% or 70.1% when initial oil content was equal to 176g/l or 440g/l.

Fourthly, we measured the reusability of the electrospun fibrous membrane, and the results are shown in Figure 18. It could be found that with increasing the times of repeated use, oil removal efficiency decreased. However, oil removal efficiency still reached 74.2% after using for seven times, thus we considered that the fibrous membrane could be used for several times during oil-water separation.

Finally, we researched the capability of the fibrous membrane to separate emulsified pump oil from water. It could be seen from Figure 19 and Figure 20 that the emulsion was a kind of homogeneous milky liquid before separation, and the liquid became clear and transparent after separation which lasted for 30min. Additionally, we adopted the extraction method mentioned above to analyze the mass of residual pump oil in the filtrate, and found out that the mass of residual pump oil in the filtrate approached 0g. The above phenomena indicated that the fibrous membrane had good interactions with emulsified pump oil and could adsorb pump oil from water when the emulsion passed.

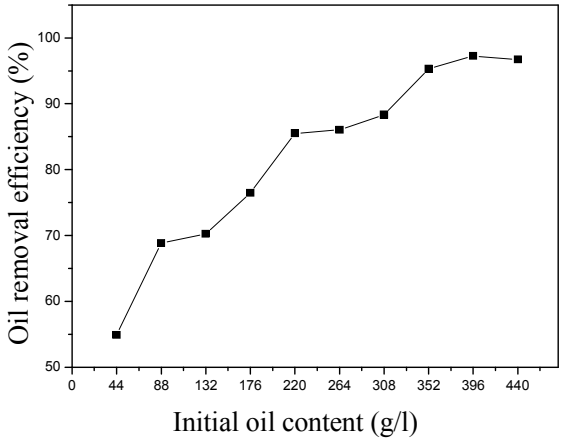


**Figure 15.** the effect of initial oil content on oil removal efficiency; the electrospun fibrous membrane 3* as the tested sample; an extrusion rate of 4ml/h and the 30ml syringe with eccentric outlet were used

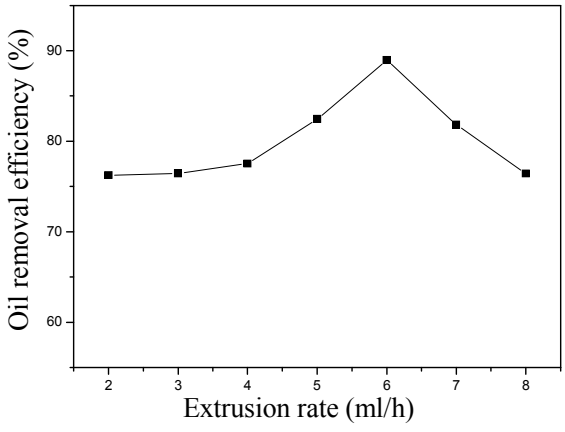


(a)

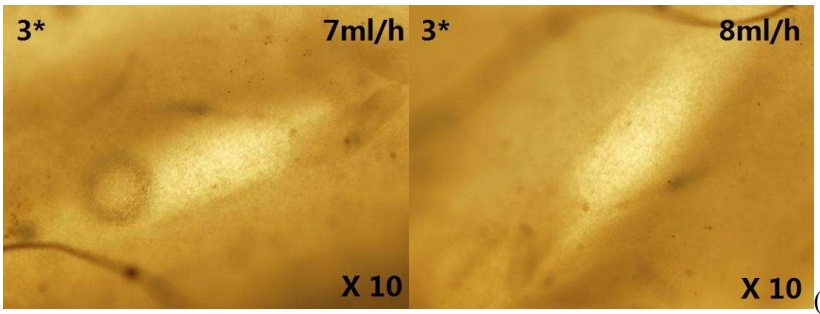


(b)

**Figure 16.** the effect of extrusion rate on oil removal efficiency (a) and polarized optical images of the membrane after separation test (b); the electrospun fibrous membrane 3* as the tested sample; an initial oil content of 176g/l and the 30ml syringe with eccentric outlet were used

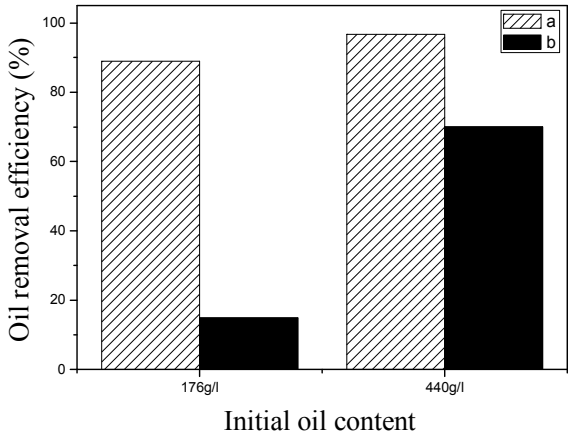


**Figure 17.** the effect of oil-water interface position on oil removal efficiency; the electrospun fibrous membrane 3* as the tested sample; an extrusion rate of 6ml/h was used; a: the 30ml syringe with eccentric outlet; b: the 30ml syringe with centered outlet

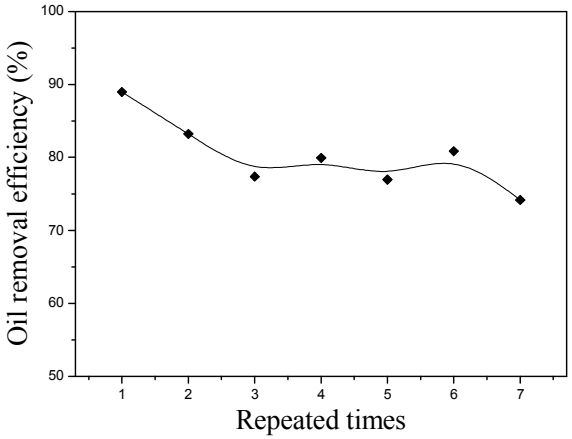


**Figure 18.** the change of oil removal efficiency with the times of repeated use; the electrospun fibrous membrane 3* as the tested sample; an extrusion rate of 6ml/h, an initial oil content of 176g/l, and the 30ml syringe with eccentric outlet were used

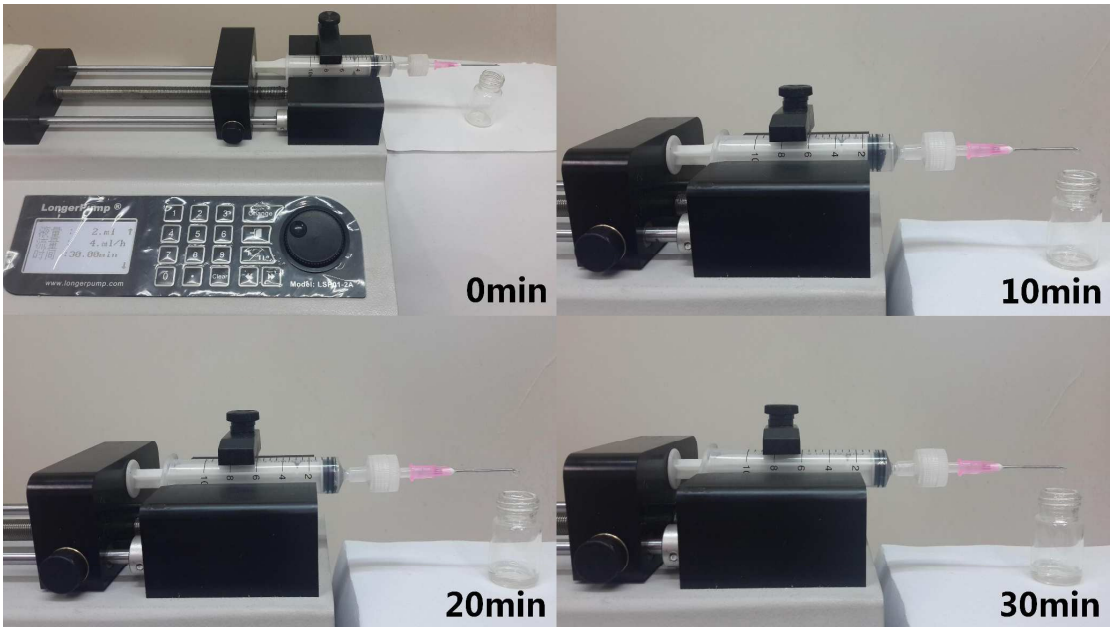


**Figure 19.** the separation of emulsified pump oil from water; the electrospun fibrous membrane 3* as the tested sample; an extrusion rate of 4ml/h and 2ml emulsion was sucked into a 10ml syringe

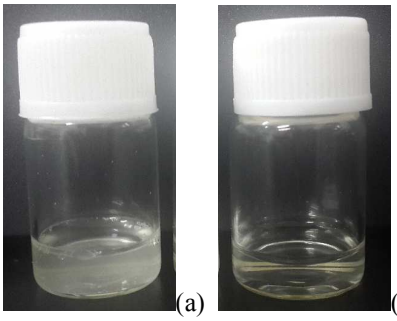


**Figure 20.** the emulsion (a) and the water after separation (b)

## Conclusions

The fibrous material prepared from the suspension polymerized resultant of styrene and butyl acrylate had better low-temperature flexibility in comparison with the polystyrene fibrous material. BA structural units existed on every fibrous membrane's surface except the polystyrene fibrous membrane's surface, and the number of BA structural units decreased with decreasing BA feed ratio. The suspension polymerized resultant of styrene and butyl acrylate was their copolymer, and the content of styrene and butyl acrylate structural units in the copolymer greatly approached the feed ratio of styrene to butyl acrylate; additionally, the thermal stability of the fibrous membrane prepared from the copolymer became bad with increasing BA feed ratio. Too much or too little BA could hardly improve the crystallinity of the suspension polymerized resultant of styrene and butyl acrylate during electrospinning, and only when a proper amount of BA was used to copolymerize with St, was their suspension polymerized resultant able to form ordered structure during electrospinning. The viscidity and elasticity of BA structural units had a great impact on the morphology of the fibrous membrane electrospun from the suspension polymerized resultant of styrene and butyl acrylate. All the fibrous membranes had good hydrophobicity and lipophilicity, exhibiting good capability to separate oil or emulsified oil from water. As initial oil content increased from 44 to 440g/l, oil removal efficiency rose gradually, and then tended to be stable. Oil removal efficiency firstly increased and then decreased with an increase in extrusion rate from 2ml/h to 8ml/h, and the highest oil removal efficiency appeared at 6ml/h, additionally, the position of oil-water interface also had a great impact on oil removal efficiency. The fibrous membranes had good reusability during oil-water separation.

## Acknowledgements

The authors acknowledge the financial supports provided by the National Nature Science Foundation of China (Project number: 51103099), Tianjin Municipal Natural Science Foundation (Project number: 12JCQNJC01600), Research Fund for the Doctoral Program of Higher Education of China (Project number: 20111201120002), and China Postdoctoral Science Foundation (Project number: 2014M550143).

## References

1 J. T. Wang, Y. Zheng and A. Q. Wang, *Chem. Eng. J.*, 2012, **213**, 1.

2 Y. Zheng, J. T. Wang, Y. F. Zhu and A. Q. Wang, *J. Environ. Sci.-China*, 2015, **27,** 21.

3 Q. F. Wei, R. R. Mather, A. F. Fotheringham and R. D. Yang, *Mar. Pollut. Bull.,* 2003, **46**, 780.

4 H. T. T. Duong and R. P. Burford, *J. Appl. Polym. Sci.*, 2006, **99**, 360.

5 M. Z. Liu, F. L. Zhan and H. S. Jiang, *Journal of Lanzhou University of Technology*, 2003, **39**, 46.

6 H. W. Xiao, *Adv. Mater. Res.*, 2012, **502**, 222.

7 Y. Feng, C. F. Xiao and N. K. Xu, *Proceedings of the 2007 international conference on advanced fibers and polymer*

*materials,* Chemical Industry Press, Beijing, 2007, **1-2**, p. 606.

8 N. K. Xu, C. F. Xiao and Y. Feng, *Polym.-Plast. Technol.*, 2009, **48**, 716.

9 N. K. Xu and C. F. Xiao, *J. Mater. Sci.*, 2010, **45**, 98.

10 J. Lin, Y. Shang, B. Ding, J. Yang, J. Yu and S. S. Al-Deyab, *Mar. Pollut. Bull.*, 2012, **64**, 347.

11 J. F. Zheng, A. H. He, J. X. Li, J. Xu and C. C. Han, *Polymer*, 2006, **47**, 7095.

12 Y. Miyauchi, B. Ding and S. Shiratori, *Nanotechnology*, 2006, **17**, 5151.

13 J. Lin, B. Ding, J. Yang, J. Yu and G. Sun, *Nanoscale*, 2012, **4**, 176.

14 H. T. Zhu, S. S. Qiu, W. Jiang, D. X. Wu and C. Y. Zhang, *Environ. Sci. Technol.*, 2011, **45**, 4527.

15 M. W. Lee, S. An, S. S. Latthe, C. Lee, S. Hong and S. S. Yoon, *ACS Appl. Mater. Inter.*, 2013, **5**, 10597.

16 B. Meng, J. J. Deng, Q. Liu, Z. H. Wu and W. Yang, *Eur. Polym. J.*, 2012, **48**, 127.

17 K. Verebélyi, Á. Szabó and B. Iván, *Polymer*, 2012, **53**, 4940.

18 W. Wang and Q. Zhang, *J. Colloid Interf. Sci.*, 2012, **374**, 54.

19 Y. Tabata and H. Abe, *Polym. Degrad. Stabil.*, 2013, **98**, 1796.

20 T. Benelli, L. Angiolini, D. Caretti, M. Lanzi, L. Mazzocchetti, E. Salatelli and L. Giorgin, *Dyes Pigments*, 2014, **106**, 143.

21 T. Pongprayoon, E. A. Yanumet N, O'Rear, W. E. Alvarez and D. E. Resasco, *J. Colloid Interf. Sci.*, 2005, **281**, 307.

22 D. Martini, K. Shepherd, R. Sutcliffe, J. Kelber, H. Edwards and R. San Martin, *Appl. Surf. Sci.*, 1999, **141**, 89.

23 Y. B. Cheng and Z. G. Wang, *Polymer*, 2013, **54**, 3047.

24 T. Nishino, Y. Urushihara, M. Meguro and K. Nakamae, *J. Colloid Interf. Sci.*, 2005, **283**, 533.

25 E. H. Lock, D. Y. Petrovykh, P. Mack, T. Carney, R. G. White, S. G. Walton and R. F. Fernsler, *Langmuir*, 2010, **26**, 885.

26 V. K. Konaganti and G. Madras, *Ind. Eng. Chem. Res.*, 2009, **48**, 1712.

27 J. P. Mahalik and G. Madras, *Ind. Eng. Chem. Res.*, 2005, 44, 4171.

28 Y. Hua, C. Chena and C. Wang, *Polym. Degrad. Stabil.*, 2004, **84**, 505.

29 S. Duquesne, J. Lefebvre, R. Delobel, G. Camino, M. LeBras and G. Seeley, *Polym. Degrad. Stabil.*, 2004, **83**, 19.

30 M. Fernandez-Garcia, J. L. de la Fuente, M. L. Cerrada and E. L. Madruga, 2002, *Polymer*, **43**, 3173.

31 N. M. Ahmad, F. Heatley and P. A. Lovell, *Macromolecules*, 1998, **31**, 2822.

32 M. Suzuki and C. A. Wilkie, *Polym. Degrad. Stabil.*, 1995, **47**, 217.

33 R. F. Ding, Y. Hua, Z. Gui, R. W. Zong, Z. Y. Chen and W. C. Fan, Polym. Degrad. Stabil., 2003, **81**, 473.

34 H. Kaczmarek, A. Felczak and A. Szalla, *Polym. Degrad. Stabil.*, 2008, **93**, 1259.

35 S. Pasupuleti and G. Madras, *Ultrason. Sonochem.*, 2010, **17**, 819.

36 H. R. Shams, D. Ghanbari, M. Salavati-Niasari and P. Jamshidi, *Compos. Part B-Eng.*, 2013, **55**, 362.

37 R. K. Balakrishnan and C. Guria, *Polym. Degrad. Stabil.*, 2007, **92**, 1583.

38 Y. H. Hu, C. Y. Chen and C. C. Wang, *Polym. Degrad. Stabil.*, 2004, **84**, 505.

39 P. Kamasa, M. Merzlyakov, M. Pyda, J. Pak, C. Schick and B. Wunderlich, *Thermochim. Acta*, 2002, **392-393**, 195.

40 Issam Thaher Amr, Adnan Al-Amer, Selvin P. Thomas, Mamdouh Al-Harthi, Salihu Adamu Girei, Rachid Sougrat and Muataz Ali Atieh, *Compos. Part B-Eng.*, 2011, **42**, 1554.

41 W. B. Yang, B. J. Zhang, Y. T. Dai, X. H. Tang and L. Zhang, *Fusion Eng. Des.*, 2008, **83**, 725.

42 L. Jiang, Y. Zhao and J. Zhai, *Angew. Chem.*, 2004, **116**, 4438.

43 Y. Miyauchi, B. Ding and S. Shiratori, *Nanotechnology*, 2006, **17**, 5151.

44 B. Ding, T. Ogawa, J. Kim, K. Fujimoto and S. Shiratori, *Thin Solid Films*, 2008, **516**, 2495.

45 T. Bharathidasan, S. Vijay Kumar, M. S. Bobji, R. P. S. Chakradhar and B. Basu, *Appl. Surf. Sci.*, 2014, **314**, 241.